Proceedings of the 9th U.S. National and 10th Canadian Conference on Earthquake Engineering
Compte Rendu de la 9ième Conférence Nationale Américaine et
10ième Conférence Canadienne de Génie Parasismique
July 25-29, 2010, Toronto, Ontario, Canada • Paper No

PLASTICITY-BASED NONLINEAR FINITE ELEMENT ANALYSIS OF REINFORCED CONCRETE COLUMNS WITH INADEQUATE SEISMIC DETAILING

E. L. Sammarco[1] and A. B. Matamoros[2]

ABSTRACT

In zones of high seismicity, properly detailed reinforced concrete columns contain adequate transverse reinforcement to resist the large shear demand associated with the development of the column's full flexural strength. Unfortunately, this capacity design methodology was not fully adopted into building codes until the early 1970's; thus rendering older reinforced concrete building columns vulnerable to premature shear failure (shear-critical) and associated loss of lateral load capacity. The fact that shear-critical columns have the potential to sustain a shear failure prior to axial failure is well established and implemented in evaluation standards such as FEMA 356 and ASCE 41. However, if the concrete core is not adequately confined, shear and axial failure are likely to occur simultaneously. This paper discusses computer simulations of three shear-critical reinforced concrete columns subjected to lateral load reversals of increasing magnitude with the intent to investigate the principal mode of failure as well as any secondary modes of failure. Results from three-dimensional nonlinear finite element models developed using the computer program ABAQUS are compared with data from three similar column assemblies tested to study the collapse risk of older reinforced concrete structures. Two of the column assemblies exhibited simultaneous shear and axial failure. Simulating the response of this type of column is a very challenging computational task due to the brittle behavior of the concrete, which results from the small amount of transverse reinforcement. A reasonable match was found between experimental and analytical response up to the point of axial failure, with the finite element model providing an accurate representation of the changes in stiffness observed during the test.

Introduction

A significant percentage of the reinforced concrete building inventory in large US population centers located in areas of high seismicity was built prior to 1970, in accordance with detailing requirements of existing building codes at the time. Significant changes to detailing practice were introduced into seismic codes in response to damage observed during the 1971 San Fernando Earthquake. As a result, a large number of older reinforced concrete buildings are

[1]Graduate Research Assistant, Dept. of Civil, Architectural, and Environmental Engineering, University of Texas at Austin, Austin, TX 78712
[2]Associate Professor, Dept. of Civil, Environmental, and Architectural Engineering, University of Kansas, Lawrence, KS, 66045

considered to have deficient detailing by modern standards. In order to evaluate the vulnerability of these buildings and to develop efficient mitigation strategies there is a need to improve the ability to simulate the nonlinear behavior of heavily damaged reinforced concrete members and estimate critical response parameters such as peak lateral and axial load capacity as well as member ductility.

This study focuses on using finite element analysis to simulate the behavior of three shear-critical columns tested to complete loss in axial load carrying capacity. This methodology was chosen because it takes into account the interaction between shear, flexure and axial load, and because developing a reliable model provides a valuable tool to study the deformation capacity of this type of column. Models of this type are particularly useful to study the response of columns subjected to bidirectional loading, which are being tested as part of a later stage of this research project. All three columns analyzed had similar detailing and material properties, with the main differences being the amount of longitudinal reinforcement and the axial load. The global response of the analytical model was calibrated based on experimental results from one of the pseudo-static column tests and evaluated based on experimental results from the remaining two.

Specimen Configuration

A detailed description of the column specimens and their behavior during the tests are presented elsewhere by Matamoros et al. (2008). The reinforced concrete column members had an 18 in. x 18 in. [457 mm x 457 mm] square cross section and a 116 in. [2,946 mm] clear height. The top and bottom beams had a 28 in. x 84 in. [711 mm x 2,134 mm] rectangular cross section and a 30 in. [762 mm] depth. The main thrust of the experimental program was to investigate the hysteretic behavior and controlling failure mode of the inadequately detailed main column member. Consequently, the top and bottom beams were conservatively proportioned to limit their contribution to the lateral deformation of the specimen. A diagram showing specimen dimensions and reinforcement details is presented in Fig. 1.

The square column section had approximately 2.5 % longitudinal steel reinforcement for columns 1 and 2 (eight No. 9 bars symmetrically placed around the perimeter of the cross section) and 3 % for column 3 (eight No. 10 bars). The cover, measured from the centerline of the steel reinforcement, was approximately 2½ in. (64 mm). The longitudinal reinforcement was developed using 90 deg. hooks extending into the top and bottom beams. Transverse reinforcement consisted of No. 3 rectilinear closed hoops spaced at 18 in. (457 mm) on center along the full height of the column. Each rectilinear hoop was developed with a 90 deg. hook and a $5d_b$ extension beyond the hook.

Material Properties

The reinforced concrete specimens were cast with normal-weight concrete. The maximum size of the coarse aggregate was ¾ in (19 mm). Mix proportions are presented elsewhere (Matamoros et al., 2008). The properties of the concrete are summarized in Table 1.

Table 1. Measured concrete properties for column specimens.

Measured Concrete Property	Column 1	Column 2	Column 3
Test Day Compressive Strength, psi (MPa)	4800 (33)	4880 (34)	2510 (17)
Modulus of Rupture, f_r, psi (MPa)	740 (5.1)	870 (5.8)	690 (4.8)
Modulus of Elasticity, E_c, ksi (GPa)	3770 (26)	3610 (25)	3270 (22)

ASTM A706 steel was used for all longitudinal bars in the column. The transverse column hoops and all of the beam reinforcement consisted of ASTM A615 steel. Tensile tests were performed on both the No. 9 and No.10 longitudinal bars and No. 3 transverse hoops, from which the average yield stresses (f_{yl}) and (f_{yt}) were determined to be 64 ksi (441 MPa) and 54 ksi (372 MPa), respectively.

Finite Element Model

As shown in Fig. 2, the finite element model of the assembly consisted of top and bottom beams, a square column section, the longitudinal steel reinforcement, and the rectilinear transverse steel reinforcement. The concrete portions of the specimen were represented using 8-noded quadratic brick elements with embedded steel reinforcement. The reinforcing bars were simulated using one dimensional truss elements.

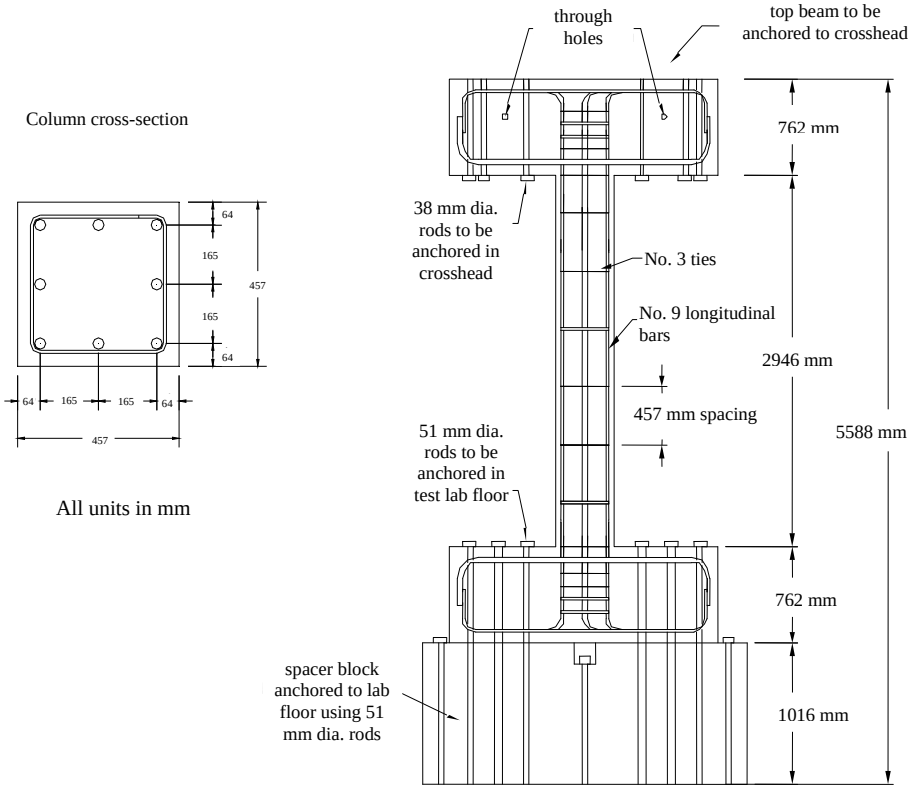

Figure 1. Specimen dimensions and detailing.

During the experimental program post-tensioned rods were used to fasten the top beam to the cross head and the bottom beam to the laboratory strong floor. These rods induced a significant amount of compression in both beams. The observed behavior of the specimens confirmed that the portions of the top and bottom beams lying outside the square column section footprint exhibited essentially linear elastic behavior throughout the tests, thus resulting in negligible cracking. Therefore, to facilitate numerical convergence and reduce computation time, these portions of the top and bottom beams were modeled using a linear-elastic concrete material model. The portion of the top and bottom beams lying inside the square column section footprint were modeled using the damage plasticity concrete material model implemented in ABAQUS. Likewise, the square column section was defined with the damage plasticity concrete material model as described later in this paper. The longitudinal and transverse steel reinforcement were defined with the linear kinematic hardening steel material model, each in accordance with their respective measured material properties.

The interaction of the concrete continuum elements with the steel truss elements was defined by employing the embedded element technique available in ABAQUS. This technique assumes perfect bond between the concrete and the steel reinforcement. This assumption is likely to result in lower estimates of lateral drift during the mid to latter stages of the cyclic load history because the bond slip phenomenon at the beam–column interface is neglected. However, experimental results suggested that, given the development length afforded by the beam depth along with the brittle response of the column, the amount of lateral deformation related to slip was relatively small. For this reason the deformation related to slip was calculated following a commonly used methodology (Matamoros, 1999) and subsequently added to the computed lateral deflection. Deformations measured at the base of the columns showed that the simple bond slip model used in this study provided accurate estimates of rotation at the base due to this effect.

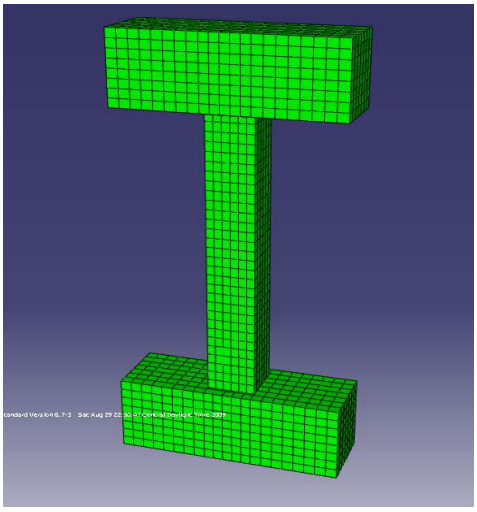

Figure 2. Finite element mesh.

The interaction of the concrete surfaces at the beam–column interfaces was modeled using contact surface properties implemented in ABAQUS. The employed interaction surface definition precluded any slip between the two contact surfaces in the tangential direction. In the normal direction, a modified “hard” contact surface property was defined such that compressive stresses were always transferred across the interface but tensile stresses were only transferred if the magnitude was below the measured modulus of rupture.

The boundary conditions of the finite element model were defined such that the bottom face of the bottom beam was restrained in all three translational DOF during all analysis steps and the top face of the top beam was constrained to the displacement–controlled loading histories defined in the various analysis steps.

Concrete Plasticity Model

The concrete damage plasticity model implemented in ABAQUS is based on the assumption of non-associated potential plastic flow. The Drucker-Prager hyperbolic flow potential function is implemented herein and can be mathematically expressed as follows:

$$G = \sqrt{(\varepsilon\, \sigma_{to}\, tan\, \psi\,)^2 + q^2} - p\, tan\psi \tag{1}$$

where σ_{to}= uniaxial stress at failure. Furthermore, the plasticity model in ABAQUS implements the yield function originally developed by Lubliner et al. (1989) and later modified by Lee and Fenves (1998) to account for different evolution of strength under tension and compression. The yield function can be mathematically expressed as follows:

$$F = \frac{1}{1-\alpha}\Big(q - 3\alpha p + \beta(\varepsilon^{pl})\sigma_{max} - \gamma(-\sigma_{max})\Big) - \sigma_c(\varepsilon^{pl}) = 0 \tag{2}$$

$$\alpha = \frac{(\sigma_{bo}/\sigma_{co})-1}{2(\sigma_{bo}/\sigma_{co})-1}\ ; \qquad 0 \le \alpha \le 0.5 \tag{3}$$

$$\beta = \frac{\sigma_c(\varepsilon^{pl})}{\sigma_t(\varepsilon^{pl})}\,(1-\alpha) - (1+\alpha) \tag{4}$$

$$\gamma = \frac{3(1-K_c)}{2K_c-1} \tag{5}$$

where, σ_{max} = maximum principal effective stress tensor, $\sigma_t(\varepsilon^{pl})$ = effective tension cohesion stress, and $\sigma_c(\varepsilon^{pl})$ = effective compression cohesion stress. Four plasticity parameters are required to completely define the damage plasticity model implemented in ABAQUS; namely, the dilation angle in the *p*-*q* plane (*p* is the effective hydrostatic stress and *q* is the Mises equivalent effective stress), Ψ, the flow potential eccentricity, ε, the ratio of initial equibiaxial compressive yield stress to initial uniaxial compressive yield stress (σ_{b0}/σ_{co}), and the ratio of the second stress invariant on the tensile meridian to that on the compressive meridian at initial yield for any given value of the pressure invariant *p* such that the maximum principal stress is negative (K_c). In order to define the aforementioned plasticity parameters, a suite of laboratory tests are required (Jankowiak and Lodygowski, 2005) including: uniaxial compression test, uniaxial tension test, biaxial plane state of stress test, and a triaxial test (superposition of the hydrostatic state of stress and the uniaxial compression stress). Because the experimental phase of this study did not include all the required laboratory tests, the plasticity parameters were calibrated based on experimental results from concrete prisms tested by Roy and Sozen (1964) which had similar concrete properties. The specimens tested by Roy and Sozen were 5 in. (127 mm) x 5 in. (127 mm) x 25 in. (635 mm) reinforced concrete prisms with various amounts of transverse and longitudinal steel reinforcement. Based on the results of this calibration study, the following plasticity parameters were adopted for this study: dilation angle Ψ= 35 deg., flow potential eccentricity ε = 0.10, biaxial stress ratio σ_{b0}/σ_{co} = 1.16, and deviatoric plane parameter K_c = 2 / 3.

Uniaxial Stress-Strain Relationship for the Concrete in Compression

The uniaxial compressive stress-strain behavior of the concrete was defined using the model proposed by Mander et al. (1988). The confined concrete compressive strength ($f`_{cc}$) for the stress-strain model was calculated based on the general solution of the multiaxial failure criterion originally defined by William and Warnke (1975). The ultimate compressive strain was calculated based on a lower bound empirical expression developed for beams by Corley (1966). According to Corley the main contributors to the ultimate compressive strain of a flexural member are the member width, the internal moment gradient, and the amount of binding reinforcement present within the member.

$$\varepsilon_u = 0.003 + 0.02\, {}^{b}/_{z} + \left(\frac{\rho" f_y}{20}\right) \qquad (6)$$

Where, b = width of structural member, z = distance between points of zero and maximum moment, ρ"= binding reinforcement ratio, and f_y = yield stress (in ksi)

Uniaxial Stress-Crack Displacement Relationship for the Concrete in Tension

The uniaxial tensile behavior was assumed to be linear elastic up to the cracking stress, and described by a modified fracture energy model beyond the cracking stress. The use of stress–strain relationships to describe the post-cracking behavior of concrete has been shown to introduce mesh sensitivity; that which impedes the ability of the results to converge to a unique solution as the mesh is refined because mesh refinement generally leads to narrower crack bands. This numerical deficiency is even more of a concern in local regions of a concrete mesh in which the concrete has small amounts of steel reinforcement. This limitation was addressed by implementing a stress–crack displacement post cracking relationship based on fracture energy concepts (Hillerborg, 1976). Theory suggests that a concrete specimen will crack at some section under tensile stresses, and its length will ultimately be determined by the opening of the crack after it has been pulled apart sufficiently for most of the stress to be removed. Thus, the post cracking model can be defined by a stress–displacement curve in which the area under the curve is equal to the fracture energy. Hillerborg concluded that a linearly descending post cracking curve was appropriate to represent the behavior of plain concrete.

The reinforced concrete column specimens contained a fair amount of longitudinal steel reinforcement, therefore it was concluded that the linearly decending post failure curve proposed by Hillerborg would not be entirely appropriate for this study. Instead, a more liberal post failure stress–crack displacement curve was utilized allowing for a greater tension stiffening effect to occur before complete tensile failure.

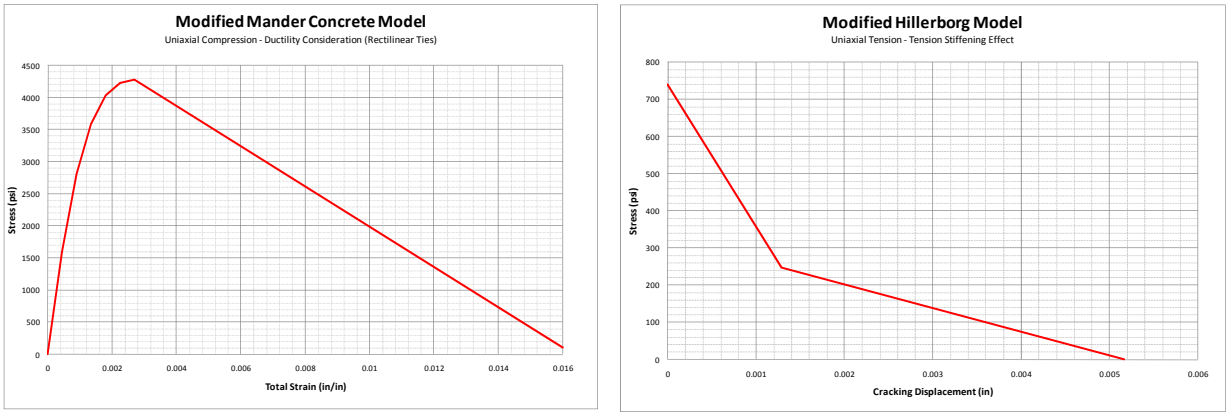

Figure 3. Concrete material models – Column 1

Damage Variables

When subjected to cyclic loading, reinforced concrete sustains progressive damage and an associated reduction in stiffness. For reinforced concrete structures located in regions of high seismicity, current design codes require that adequate confining reinforcement be provided in columns to protect the concrete core from excessive damage, and to prevent buckling of the longitudinal reinforcement. The presence of core confinement allows a well detailed column to carry axial load even after a primary shear failure. The main objective of this study, however, was to investigate the behavior of reinforced concrete columns detailed according to codes that pre-date the 1971 San Fernando Earthquake. Because significant damage and stiffness degradation were anticipated, stiffness degradation and stiffness recovery variables were utilized in the damage plasticity model. The stiffness degradation variables d_c and d_t implemented in the damage plasticity model of ABAQUS are scalar values that depend on material response quantities such as inelastic compressive strain or tensile crack displacement. As the post-peak compressive stress or tensile crack displacement increases the material experiences non-recoverable damage, and the stiffness of the material degrades after a load reversal takes place. This stiffness degradation phenomenon is simulated computationally by reducing the initial elastic modulus. The compression stiffness degradation variable is generally defined by an exponentially decaying function dependent on a particular field variable. Total compression degradation was not considered in this study due to anticipated numerical convergence issues.

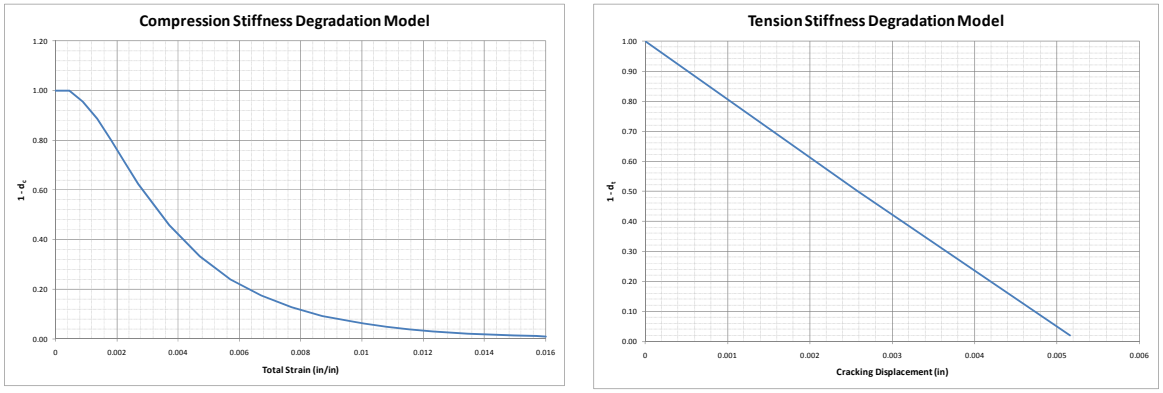

Figure 4. Damage Model Parameters.

In this study, the compression stiffness degradation variable was defined by an exponential function dependent on the plastic component of compressive strain.

$$d_c = 1 - e^{-300\,\varepsilon^{pl}} \tag{7}$$

where ε^{pl} = plastic component of compressive strain. In addition, the compression stiffness recovery variable was taken to be unity (w_c = 1.0) which implies that as cracks close during load reversal the compression stiffness is completely recovered. The tension stiffness degradation variable was defined by a linear expression in which a 50 percent reduction in elastic stiffness was assumed to have taken place when the critical crack bandwidth value was reached and 98 percent when twice the critical crack bandwidth value was reached. The tension stiffness recovery variable was taken to be zero (w_t = 0).

Reinforcing Steel Plasticity Model

A pressure-independent metal plasticity model was used to approximate the cyclic behavior of the ductile steel reinforcement. The metal plasticity model assumes linear kinematic hardening (constant hardening modulus), an equivalent Mises yield surface, and associated plastic flow. In addition, the ratio of plastic modulus to elastic modulus was assumed to be 0.02. The fundamental stress–strain curves for the longitudinal and transverse steel reinforcement were assumed to be bilinear. One of the major benefits of employing this type of metal plasticity model is that it provides the ability to analytically capture the Bauschinger effect as the reinforcing steel undergoes multiple load cycles.

Analysis and Solution Techniques

Analysis Steps

The entire analysis regime consisted of three separate "general static" analysis steps; namely, the initial step, the axial step, and the lateral step. The initial step, required by ABAQUS, was used merely to define the bottom beam boundary conditions and activate the contact surface definitions. The axial step initiated a gravitational field as well as applied the prescribed constant axial compressive force to the top of the specimen by means of a uniform vertical displacement. The vertical displacement was derived based on the desired axial compressive force along with the elastic axial stiffness of the column. The axial compressive force was held constant throughout the remainder of the analysis regime. During the lateral step an amplitude function, defined by the lateral load protocol shown in Figure 5, was tied to the lateral DOF of the top surface nodes of the top beam. The application of the amplitude function to the top boundary conditions induced displacement – controlled cyclic lateral loading. The successful completion of the lateral analysis step defined the end of the analysis regime.

Figure 5. Displacement Protocol.

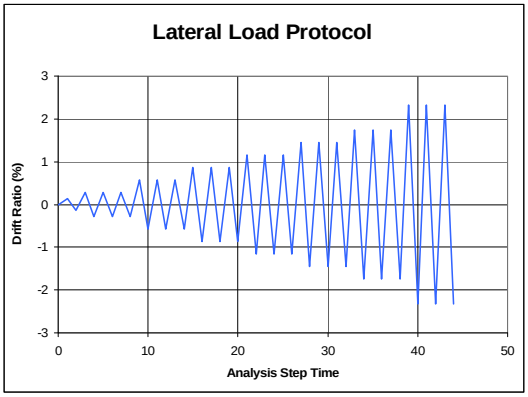

Solution Algorithm

An implicit solution algorithm was implemented during this study. In particular, the Newton-Raphson method was used to calculate the response of the columns. An adaptive numerical stabilization technique was implemented during the analysis to mitigate local numerical instabilities and aid in solution convergence. Analyses involving significant material plasticity in localized regions of the finite element model may experience numerical instabilities and convergence difficulties. In ABAQUS this potential problem can be mitigated by introducing artificial damping forces of very small magnitude to help avoid excessive element distortion and numerical ill-conditioning. The application of small damping forces is the underlying concept behind the adaptive stabilization technique. It should be noted that excessive amounts of artificial damping can lead to a gross imbalance of system energy which in turn will yield erroneous analysis results. For this reason care was taken in the implementation of this technique to ensure accurate and meaningful analysis results.

Visco-Plastic Regularization

During the experimental program significant material plasticity and associated damage was observed near the beam–column interfaces where the greatest moment demand existed. This localized and highly plastic material response lends itself to potential numerical convergence issues in a nonlinear finite element analysis. As such, visco-plastic regularization was incorporated into the concrete material model definition in order to mitigate this potential convergence problem. Regularizing the concrete damage plasticity model using visco-plasticity allows stresses to breach the yield surface boundary. The Duvaut-Lions regularization methodology was utilized herein where the visco-plastic strain rate tensor and viscous stiffness degradation variable are expressed as follows, respectively.

$$\varepsilon'_v{}^{pl} = \frac{1}{\mu}\left(\varepsilon^{pl} - \varepsilon_v{}^{pl}\right) \tag{8}$$

$$d'_v = \frac{1}{\mu}(d - d_v) \tag{9}$$

where μ = viscosity parameter, ε^{pl} = plastic strain evaluated in the inviscid backbone model, and d = damage variable in the inviscid backbone model. The viscosity parameter represents the relaxation time of the visco-plastic system. Furthermore, the solution of the visco-plastic system relaxes to that of the inviscid case as the ratio of the characteristic time increment of the analysis step to the viscosity parameter approaches infinity. Therefore, implementing a small viscosity parameter magnitude relative to the characteristic time increment of the analysis step generally improves the rate of convergence of the nonlinear analysis without compromising the accuracy of the results. Conversely, abusing the regularization technique by using a relatively large viscosity parameter can lead to grossly inaccurate results. In general, an appropriate viscosity parameter magnitude depends upon the analysis to be conducted as well as the anticipated amount and spread of plasticity (localized versus global).

Simulation Results

The simulation parameters of the finite element model were calibrated to provide accurate estimates of the peak lateral force and peak lateral drift ratio at failure for column 1. A detailed description of the progression of damage of the three specimens is presented by Matchulat (2008). The model also provided a good representation of the observed mode of failure (simultaneous shear and axial failure).

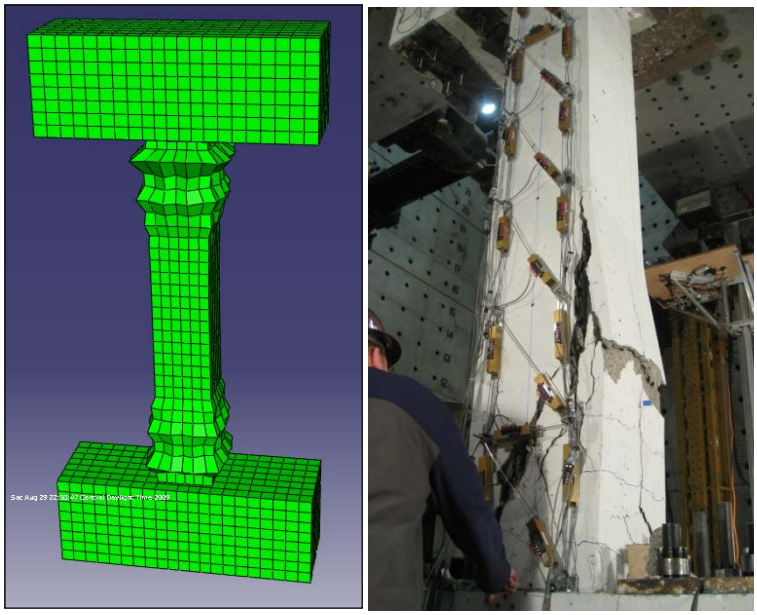

Figure 6. (a) Deformed Shape near failure (b) Actual Column

This mode of failure presented a complex computational challenge. Figure 6a shows the deformed shape of the simulated column at failure next to a photograph of the actual specimen. The deformed shape shows areas of severe damage in the regions of maximum moment, which is consistent with the observed behavior.

Figure 7a shows a comparison of the calculated and measured hysteresis curves for column 1. The analytical model provided an accurate estimate of the peak lateral load of approximately 90 kips and a loss of lateral load carrying capacity at a lateral drift ratio of approximately 1.00%. The brittleness of the simultaneous shear and axial failure is quite apparent from the photograph in Figure 6b and the experimental curve in Fig. 7a. The sudden drop in stiffness at a drift ratio of approximately -1% corresponds to axial load failure. It should be noted that a "sudden" axial failure was not captured in the computer simulations. Rather, a macroscopic softening effect was observed beginning at a drift ratio of approximately 1.00%. This discrepancy between the experimental and analytical results is a consequence of the modeling techniques that had to be implemented in order to achieve numerical convergence at axial failure. It is postulated that the inclusion of an element erosion technique may have ameliorated the failure response of the computer simulations. The model used to analyze column 1 was subsequently modified to perform simulations for columns 2 and 3. Column 2 was identical to column 1 with the exception of a lower axial load of 340 kips. Column 3 was delivered the same axial load as column 1; however it contained a higher longitudinal reinforcement ratio of 3%. The same analysis parameters used in the column 1 model were used for the simulations of columns 2 and 3. The results are presented in Fig. 8a and b. The graphs show that the simulations provided an accurate estimate of the peak lateral force and associated peak lateral deformation as well as the drastic change in stiffness caused by the secondary axial failure of the column.

Conclusions

A plasticity-based analytical model was successfully implemented to calculate the lateral load and deformation capacity of reinforced concrete columns at axial failure. The analytical model was verified with a series of shear-critical column tests that experienced a secondary axial failure.

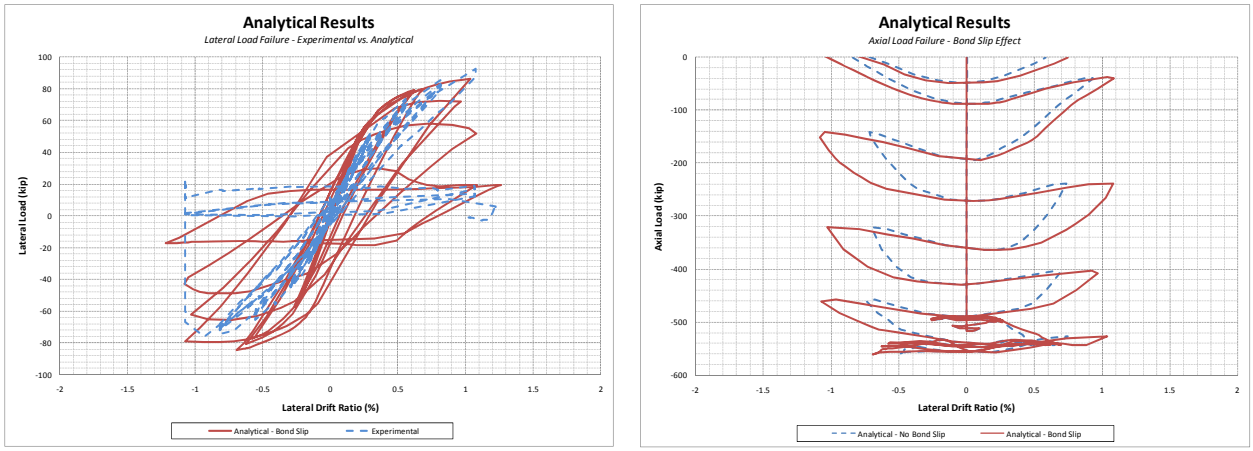

Figure 7. (a) Comparison of experimental and calculated hysteretic response for column 1 (b) Bond slip effect on analytical axial load versus lateral drift ratio response

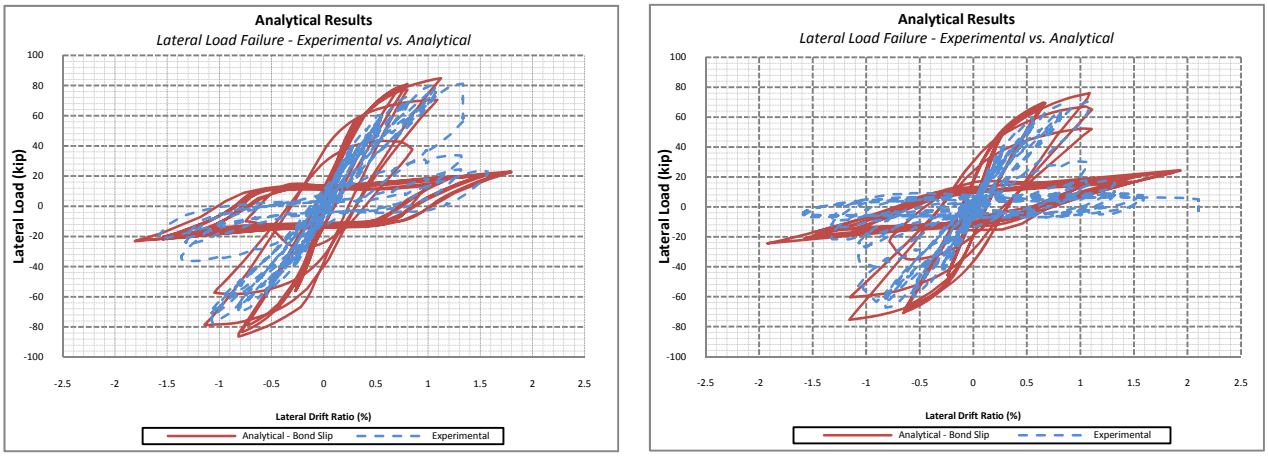

Figure 8. (a) Comparison of experimental and calculated hysteretic response for column 2 (b) Comparison of experimental and calculated hysteretic response for column 3.

Based on the results of this study, it is concluded that the model presented herein is well suited to conduct preliminary investigations on the behavior of shear-critical columns with high levels of axial load, to gain a better understanding of the parameters that influence the deformation capacity of this type of column, and/or to evaluate possible retrofit measures. This model constitutes a first step in developing high resolution simulations of columns that are expected to fail in shear and understanding how and when that failure precipitates a secondary axial failure. Further validation will be conducted upon completion of the experimental program.

The calculated column responses shown in Figures 7 and 8 represented the measured responses very well, and the observed mode of failure was captured by the computational model; although in a less brittle manner. This is one limitation of the plasticity-based concrete material model and nonlinear solution technique implemented in this study. The sudden brittle failure of the column specimen constitutes a large response discontinuity, and during severe discontinuities it is very difficult to obtain convergent numerical solutions. Numerical techniques such as visco-plastic regularization and adaptive stabilization were implemented in the analyses to mitigate the problem posed by severe response discontinuities. Another consequence of the numerical techniques utilized during this study was the resulting widths of the calculated hysteretic loops shown in Figures 7 and 8 relative to the observed values. A less conservative definition and evolution of the progressive concrete damage would have yielded narrower hysteretic loops, closer to those observed during the experimental program. However, a more aggressive definition of concrete damage would have resulted in more severe numerical convergence issues.

Acknowledgments

This work was supported primarily by the National Science Foundation under award number # 0618804 through the Pacific Earthquake Engineering Research Center (PEER). Any opinions, findings, and conclusions or recommendations expressed in this material are those of the author(s) and do not necessarily reflect those of the National Science Foundation.

References

Belarbi, A. and Hsu, T., 1994. "Constitutive Laws of Concrete in Tension and Reinforcing Bars Stiffened by Concrete." *ACI Structural Journal* 91 (4), 465-474.

Boresi, A. and Schmidt, R., 2003. *Advanced Mechanics of Materials*, John Wiley & Sons Inc.

Cofer, W., 1999. "Documentation of Strengths and Weaknesses of Current Computer Analysis Methods for Seismic Performance of Reinforced Concrete Members." *Pacific Earthquake Engineering Research Center*, PEER Report 1999/07, University of California, Berkeley.

Corley, G., 1966. "Rotational Capacity of Reinforced Concrete Beams." *ASCE Structural Journal* 92 (ST5), 121-146.

Hognestad, E., 1952. "Inelastic Behavior in Tests of Eccentrically Loaded Short Reinforced Concrete Columns." *Journal of the American Concrete Institute* 24 (2), 117-139.

Jankowiak, T. and Lodygowski, T., 2005. "Identification of Parameters of Concrete Damage Plasticity Constitutive Model." *Foundations of Civil and Environmental Engineering*, Publishing House of Poznan University of Technology, 6, 53-69.

Lee, J. and Fenves, G., 1998. "Plastic-Damage Model for Cyclic Loading of Concrete Structures." *Journal of Engineering Mechanics*, 124 (8), 892-900.

Lubliner, J., Oliver, J., Oller, S., and Onate, E., 1989. "A Plastic-Damage Model for Concrete." *Int. J. Solids and Struct.*, 25 (3), 299-326.

Mander, J., Priestley, M., and Park, R., 1988. "Theoretical Stress-Strain Model for Confined Concrete." *ASCE Journal of Structural Engineering*, 114 (8), 1804-1826.

Matamoros, Adolfo B., 1999. “Study of Drift Limits for High-Strength Concrete Columns”. *PhD Dissertation*, University of Illinois at Urbana-Champaign.

Matamoros, A., Matchulat, L., and Woods, C., 2008. “Axial Load Failure of Shear Critical Columns Subjected to High Levels of Axial Load,” 14th World Conference on Earthquake Engineering, Beijing, China, October 2008.

Matchulat, L., 2008. “Mitigation of Collapse Risk in Vulnerable Concrete Buildings.” *MS Thesis*, University of Kansas.

Roy, H., and Sozen, M., 1964. “Ductility of Concrete.” *Flexural Mechanics of Reinforced Concrete*, ACI/ASCE SP12, 213-235.

Sezen, H., 2002. “Seismic Behavior and Modeling of Reinforced Concrete Building Columns.” *Doctoral Dissertation*, University of California, Berkeley.

Simulia, 2007. “ABAQUS Analysis User’s Manual.” Version 6.7-3, Dassault Systems.

William, K. and Warnke, E., 1975. “Constitutive Model for the Triaxial Behavior of Concrete.” *International Association for Bridge and Structural Engineering* 19, 1-30.